van der Waals normal form for a one-dimensional hydrodynamic model

C. Cartes,[1] M. G. Clerc,[2] and R. Soto[2]
[1]*Facultad de Física, Pontificia Universidad Católica de Chile, Casilla 306, Santiago, Chile*
[2]*Departamento de Física, Facultad de Ciencias Físicas y Matemáticas, Universidad de Chile, Casilla 487-3, Santiago, Chile*
(Received 27 September 2003; revised manuscript received 8 April 2004; published 16 September 2004)

Phase separation in a fluidized granular system is studied. We consider a one-dimensional hydrodynamic model that mimics a two-dimensional fluidized granular system with a vibrating wall and without gravity, which exhibits a phase separation. Close to the critical point, by means of an adiabatic elimination of the temperature, we deduce the van der Waals normal form, which is the equation that describes the slow dynamics of the system and predicts the qualitative behavior in different regions of parameters. This allows us to understand the origin of the effective viscosity and the spatial saturation at the onset of the bifurcation. The hydrodynamic model and van der Waals normal form exhibit a behavior similar to the one observed in molecular dynamics simulations.

DOI: 10.1103/PhysRevE.70.031302 PACS number(s): 45.70.−n, 05.45.−a, 64.75.+g

I. INTRODUCTION

Recently, it has been shown that a fluidized granular system in two spatial dimensions with a vibrating wall and without gravity exhibits a phase separation [1–3], analogous to the spinodal decomposition of the gas-liquid transition in the van der Waals model [4]. Molecular dynamics simulations of a granular system at the onset of phase transition reveal a rich dynamical behavior characterized by the appearance, coalescence, and disappearance of bubbles. The mechanism of this phase separation is triggered by a negative compressibility implied by the fact that the granular temperature is a decreasing function of the density for a fixed geometry and boundary conditions [5]. The microscopic model used in the molecular dynamics simulations is the inelastic hard sphere (IHS) model [5–7], where grains are modeled as smooth rigid disks characterized by a constant normal restitution coefficient α. These grains have only translational degrees of freedom and there is no tangential friction between them at collisions. The inelastic hard sphere model has been widely studied and reproduces quite well many of the observed phenomena in granular fluids at moderate densities, when rotation is not fundamental (see, for example, [5–7]).

A continuous or macroscopic description of granular flows is still an open question. There are several models with different approximation schemes that produce different hydrodynamic models [8–15]. Nevertheless, using simple generic arguments, independent of the specific macroscopic model, we have shown that a fluidized granular system that exhibits phase separation can be described, close to the critical point, in good detail by the *van der Waals normal form* (VDWNF) [3]. Our previous derivation, however, was unable to predict the position of the critical point nor the values of the different coefficients appearing in the equation.

The aim of this article is to achieve an explicit derivation of the VDWNF from a hydrodynamic model. The model we will consider is an effective one-dimensional description of a two-dimensional system with a vibrating wall and without gravity. We show that when the hydrodynamic model presents an effective negative compressibility, close to the critical point of the instability, the temperature can be adiabatically eliminated in favor of the density and momentum fields. This results in a simpler model for the density and momentum that, after scaling the variables, yields the VDWNF. The procedure allows us to compute the various coefficients that appear in the VDWNF in terms of the parameters of the hydrodynamic model and to understand the physical mechanism that produces the effective viscosity and the spatial saturation in the VDWNF. We peruse the dynamics of the normal form and compare it with the dynamic behavior of the one-dimensional hydrodynamic model. Close to the instability, qualitative and quantitative agreement is observed between the VDWNF and the one-dimensional hydrodynamic model. Furthermore, far from the critical point a similar dynamic behavior is observed.

II. HYDRODYNAMIC MODEL

We consider a two-dimensional system of grains placed in a horizontal box with large aspect ratio $L_x/L_y \gg 1$, where L_x and L_y are the lengths of the box (see Fig. 1). The grains move without friction in the box. For the sake of simplicity henceforth, we will refer to horizontal x and vertical y directions as the long and short directions, respectively. The system is periodic in the long direction. The top wall reflects grains elastically while the bottom one injects energy into the system by means of vertical sinusoidal vibrations that are modeled by a thermal wall at a fixed temperature T_W. That is, each time a particle collides with the wall, it emerges with a

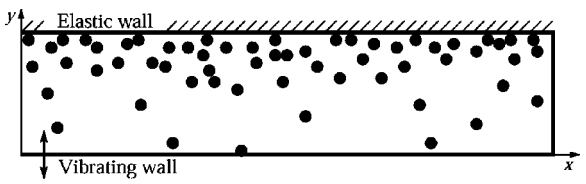

FIG. 1. Schematic representation of the system studied. Grains are placed in a horizontal box. The bottom wall is vibrating while the top one reflects grains elastically. The system is periodic in the x direction.

normal velocity taken from a thermal bath at temperature T_W. The collisions with the walls are elastic with no tangential friction, thus conserving horizontal momentum. We define the granular temperature, as in molecular fluids, to be proportional to the kinetic energy per particle in the reference frame of the fluid.

In a traditional hydrodynamic approach, the system is described by a set of macroscopic quantities: particle number density $n(x,y,t)=\langle\Sigma_i\ \delta(\vec{r}-\vec{r}_i(t))\rangle$, macroscopic velocity flow $U(x,y,t)=n^{-1}\langle\Sigma_i\ \vec{v}_i\delta(\vec{r}-\vec{r}_i(t))\rangle$, and temperature $T(x,y,t)=n^{-1}\langle\Sigma_i\ \frac{1}{2}[v_i-U(x,y,t)]^2\delta(\vec{r}-\vec{r}_i(t))\rangle$, where $\vec{r}=(x,y)$ is the position vector and $\langle\ \rangle$ represents a coarse grained average over a small region of space or time.

Starting from kinetic theory, it is possible to derive a set of equations based on mass, momentum, and energy balances [11,12,15]. The macroscopic variables have a y dependence that varies faster than the x dependence, due to the large aspect ratio of the box. Hence one can describe this system with y-averaged variables

$$\rho(x,t)=\frac{1}{L_y}\int dy\ n(x,y,t), \tag{1}$$

$$u(x,y)=\frac{1}{L_y}\int dy\ U(x,y,t), \tag{2}$$

$$\Theta(x,t)=\frac{1}{L_y}\int dy\ T(x,y,t), \tag{3}$$

and deduce a set of equations based on mass, momentum, and energy balances. Due to the y dependence of the particle number density and temperature at equilibrium, this set of equations can be nonlocal, and its study is arduous.

In order to have a simple hydrodynamic model that mimics the granular system in two spatial dimensions, we write down balance equations for the one-dimensional variables [16], which resemble those of a real two-dimensional system. Mass balance is exact, and in the momentum balance we consider pressure and viscous transfer. The energy equation is subtler because energy is not conserved due to the inelastic collisions and the energy injection at the base. We consider the usual terms in the energy equation (heat flux and mechanical work) plus one term that takes into account the local energy dissipation and injection. The system is modeled by

$$\partial_t\rho=-\partial_x(\rho u), \tag{4}$$

$$\rho\partial_t u+\rho u\partial_x u=-\partial_x P(\rho,\Theta)+\partial_x(\eta\Theta^{1/2}\partial_x u),$$

$$\rho\partial_t\Theta+\rho u\partial_x\Theta=\partial_x(C_2\partial_x\Theta^{3/2})-C_1P\partial_x u-qC_3\rho^2[\Theta^{3/2}-F^{3/2}(\rho,\lambda)]+\eta\Theta^{1/2}(\partial_x u)^2.$$

The coefficients C_1, C_2, C_3, and η are the effective one-dimensional transport coefficients that result on the projection of the two-dimensional system, which is inhomogeneous in the short direction, in one dimension. Therefore, they will depend on the geometry and the energy injection mechanisms. Furthermore, the two-dimensional transport coefficients for dense systems are elaborate functions of the density [15]. As a result, the effective one-dimensional coefficients are complex functions of the density, and we will consider them as unknown functions. Nevertheless, a precise knowledge of their values is not necessary to deduce the van der Waals normal form as long as they remain positive. The dependence of the transport coefficients on different powers of Θ is extracted from the expressions for the transport coefficients for hard spheres, but it can also be deduced by simple dimensional analysis. Finally, η is the effective viscosity, C_1 gives account of the heat production due to mechanical work, C_2 is the effective thermal conductivity, C_3 gives the energy dissipation rate, q is the inelasticity coefficient $q=(1-\alpha)/2$, α is the restitution coefficient, and $P(\Theta,\rho)$ is the pressure for a fluid of hard disks and its constitutive relation is [17]

$$P(\rho,\Theta)=\frac{(1+\rho^2/8)}{(1-\rho)^2}\rho\Theta. \tag{5}$$

The pressure of the two-dimensional granular system is a function of the number density and the temperature. When one reduces the dynamics to the y-average variables, the pressure depends nonlocally on these variables. The use of the local hard-disk equation of state (5) is a strong simplification because P is the average pressure, which does not need to satisfy the equation of state in terms of the average density and temperature. However, this simplification allows us to tackle the problem without going into the full two-dimensional system. It is important to note that the pressure diverges at the area fraction $\rho=1$. Physically, this density is unattainable because the maximum area fraction corresponds to the close packing $\rho_{CP}=\pi/2\sqrt{3}$. The equation of state gives an increasing pressure as a function of density for a given temperature.

The heat source that accounts for the energy injected by the vibrating wall is written in such a form that the homogeneous equilibrium temperature for a given density is

$$\Theta_0=F(\rho_0). \tag{6}$$

In molecular dynamic simulations of the IHS model, the average temperature Θ_0 is obtained as a function of the density for some values of the inelasticity coefficient q (see Fig. 2). For fixed inelasticity q, geometry, and boundary conditions, the equilibrium temperature is a decreasing function of density; this is so because when the density increases the number of collisions per unit time rises, and hence the dissipation grows [5]. Also, on increasing the value of q, the equilibrium temperature decreases. To model this, we have chosen the function F, plotted in Fig. 2, to be

$$F(\rho,\lambda)=\frac{e^{-\lambda\rho}(1-\rho)}{(1+\rho^2/8)}. \tag{7}$$

It is a decreasing function of the density that vanishes at $\rho=1$, since for this density all the energy is dissipated instantaneously. The parameter λ is a control parameter that takes into account the balance between the energy injection and dissipation (it plays the role of the inelasticity coefficient q). The heat source function F has been chosen by this expres-

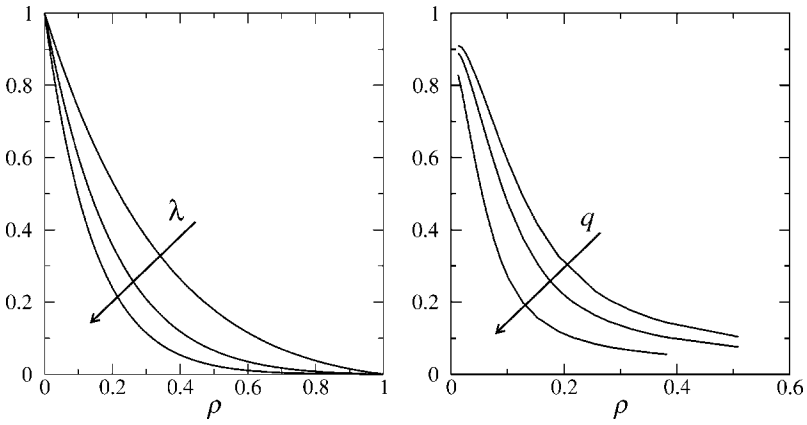

FIG. 2. Left: The heat source function F plotted against the density for $\lambda=2.0$, $\lambda=4.0$, and $\lambda=6.0$. Right: Average temperature obtained in molecular dynamics simulations for $q=0.0030$, $q=0.0046$, and $q=0.0100$. The wall temperature is $T_W=1$ and $L_y=100$.

sion because it keeps the qualitative features of the computed value and allows for a complete analysis of the hydrodynamic equations. More complex expressions for $F(\rho)$ that better fit the simulation results will produce qualitatively the same results as the expression we propose.

III. VAN DER WAALS INSTABILITY

The above model has trivial homogeneous stationary solutions $\rho=\rho_0$, $u=0$, and $\Theta=F(\rho_0)$, which represent the granular system in a homogeneous fluidized state. Note that the family of homogeneous solutions is parametrized by ρ_0, which is fixed by the initial condition. In order to study the stability of this state, we introduce the variables $\rho=\rho_0+\overline{\rho}(x,t)$, $u=v(x,t)$, $\Theta=F(\rho_0)+\theta(x,t)$ and we linearize Eqs. (4) about this homogeneous solution:

$$\partial_t\overline{\rho}=-\rho_0\partial_x v,$$

$$\rho_0\partial_t v=-\partial_x\left[P(\rho_0,F(\rho_0))+\left.\frac{\partial P}{\partial\rho}\right|_{\rho_0}\overline{\rho}+\left.\frac{\partial P}{\partial\Theta}\right|_{F(\rho_0)}\theta\right]+\eta_0 F(\rho_0)^{1/2}\partial_{xx}v,$$

$$\rho_0\partial_t\theta=-C_{10}P(\rho_0,F(\rho_0))\partial_x v+\frac{C_{20}}{F(\rho_0)^{-1/2}}\partial_{xx}\theta-q\frac{C_{30}}{F(\rho_0)^{-1/2}}\rho_0^2\left(\theta-\left.\frac{\partial F}{\partial\rho}\right|_{\rho_0}\overline{\rho}\right),\tag{8}$$

where $\eta_0=\eta(\rho_0)$, $C_{10}=C_1(\rho_0)$, $C_{20}=C_2(\rho_0)$, and $C_{30}=C_3(\rho_0)$.

By looking for solutions of the form $\overline{\rho}(x,t)=\overline{\rho}e^{\sigma t+ikx}$, $v(x,t)=ve^{\sigma t+ikx}$, $\theta(x,t)=\theta e^{\sigma t+ikx}$, it is possible to obtain the spectrum $(\sigma(k))$ of the linear perturbations. Figure 3 shows the real part of the spectrum as a function of the wave number. Neglecting the viscous term and considering small wave numbers k, the eigenvalues take the form

$$k\sqrt{-\left.\frac{dP(\rho,F(\rho))}{d\rho}\right|_{\rho_0}},\quad -k\sqrt{-\left.\frac{dP(\rho,F(\rho))}{d\rho}\right|_{\rho_0}}$$

$$-\frac{qC_{30}\rho_0}{F(\rho_0)}-k^2\left[\frac{C_{20}}{F(\rho_0)^{-1/2}}+\frac{\partial P}{\partial\theta}\left(\frac{1}{qC_{30}}-\frac{F(\rho_0)^{1/2}C_{10}}{C_{20}\rho_0^2}\right)\right].\tag{9}$$

From the previous expressions one can see that if the *effective pressure* $P(\rho,F(\rho))$ is a decreasing function of ρ_0 (negative compressibility coefficient) the trivial homogeneous state is unstable (has positive eigenvalues). The effective pressure has the form

$$P(\rho,F(\rho))=P_0\frac{e^{-\lambda\rho}}{(1-\rho)}\rho.\tag{10}$$

When $\lambda<4$ the effective pressure is an increasing function of the density, when $\lambda=4$ the effective pressure has an inflection point at $\rho=1/2$, and for $\lambda>4$ the effective pressure is a nonmonotonic function of the density as show in Fig. 4. Hence, the trivial homogeneous state is unstable (cf. Fig. 3). A classical example of this behavior is the van der Waals equation of state [4]: when the compressibility is negative ($\rho\partial P/\partial\rho<0$), the homogeneous state is unstable and the system presents a spinodal decomposition into gas and liquid phases. In model (4) this phase transition is between two granular fluid phases with different densities.

Close to the critical point, the spectrum of the homogeneous state is characterized by one branch that is separated

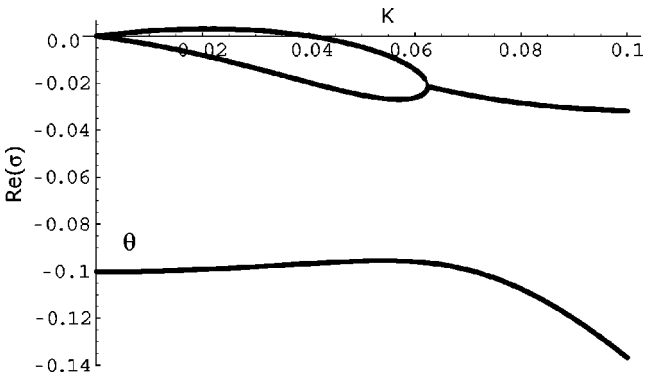

FIG. 3. Real part of the spectrum [Re(σ)] of the homogeneous solution $\rho=\rho_0$, $u=0$, and $\Theta=F(\rho_0)$ for $\rho_0=0.5$, $\alpha=5.0$, $P_0=1.0$, $\eta_0=0.0$, $C_{10}=1$, $C_{20}=1$, and $C_{30}=0.04$. The lowest branch corresponds to the temperature mode.

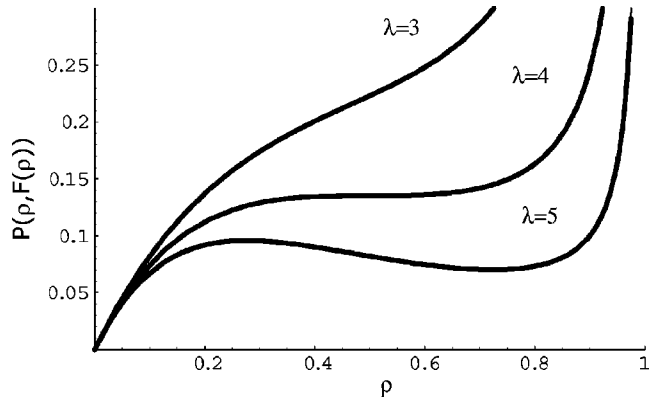

FIG. 4. Effective pressure $P(\rho,F(\rho))$ as a function of the density for different values of λ. For $\lambda<4$ the pressure is a monotonic function. When $\lambda=4$ the pressure has an inflection point at $\rho=0.5$ and for $\lambda>4$ the pressure is a nonmonotonic function.

from the others as shown in Fig. 3. Accordingly, a perturbation of the homogeneous state is characterized by a mode that is attenuated, that is, this mode varies fast and follows the dynamics driven by the other two modes, and hence this mode is a slave variable. The central manifold, i.e., the set of modes that govern the dynamics for long times, is of dimension 2. In conclusion one can remove one variable adiabatically and find a minimal description of the instability [18].

IV. VAN DER WAALS NORMAL FORM

In order to have a minimal description close to the critical point it is necessary to remove adiabatically the temperature which, to linear order, is an attenuated mode (cf. Fig. 3). If we consider that the spatial variations are small, close to the critical point the temperature can be expressed as

$$\Theta(\rho,v) = F(\rho_0+\overline{\rho},\lambda=4+\varepsilon) + \Theta_1\partial_{xx}\overline{\rho} + \Theta_2\partial_x v + \text{h.o.t.}, \tag{11}$$

where ε is the bifurcation parameter, while Θ_1 and Θ_2 are constants. The higher order terms (h.o.t.) represent linear or nonlinear terms in $\overline{\rho}$ and v and their spatial derivatives. These terms are negligible with respect to the above terms as we see later. Substituting the above ansatz into the third equation of [4] and using the other two equations yields

$$\Theta_1 = \frac{C_{20}\left.\dfrac{\partial F}{\partial\rho}\right|_{\rho_0}}{q\rho_0^2 C_{30}}, \tag{12}$$

$$\Theta_2 = -\frac{2\left(C_{10}P(\rho_0,F(\rho_0)) - \rho_0^2\left.\dfrac{\partial F}{\partial\rho}\right|_{\rho_0}\right)}{3q\rho_0^2 C_{30}F(\rho_0)^{-1/2}}. \tag{13}$$

It is important to remark that these coefficients are negative when the heat source $F(\rho,\lambda)$ is a decreasing function of the density. The physical interpretation of the term proportional to Θ_1 in the approach (11) is that when the gradients increase the temperature increases. This term produces similar effects as a surface tension. The term proportional to Θ_2 is interpreted as the temperature generated by the mechanical work, i.e., this term accounts for the transfer of mechanical to thermal energy.

Considering the critical density and the parameters around the instability ($\rho_0=1/2$ and $\lambda=4+\varepsilon$,), introducing the change of variable $\rho=1/2+\overline{\rho}(x,t)$, $u=v(x,t)$, and substituting the above temperature expansion in the second Eq. (4), at dominant order in ϵ one obtains

$$\partial_t\overline{\rho} = -\frac{\partial_x v}{2},$$

$$\frac{\partial_t v}{2} = -\partial_x\left[-\frac{\varepsilon}{e^2}\overline{\rho} + \frac{16}{3e^2}\overline{\rho}^3 + \frac{33\Theta_1}{16}\partial_{xx}\overline{\rho} + \frac{33\Theta_2}{16}\partial_x v\right] + \frac{33}{16e^2}\eta_0\partial_{xx}v. \tag{14}$$

Note that the coefficient $\frac{33}{16}(\eta_0/e^2+\Theta_2)$ is the effective viscosity. The term proportional to $33\Theta_1/16$ represents the increase of pressure with increasing gradients, which is responsible for the saturation at large wave number. Using the expression of the heat source (7) in the coefficients Θ_1 and Θ_2 and combining Eqs. (14), one obtains

$$\partial_{tt}\overline{\rho} = -\partial_{xx}\left[-\frac{\varepsilon}{e^2}\overline{\rho} + \frac{16}{3e^2}\overline{\rho}^3 - 3.31\frac{C_{20}}{qC_{30}}\partial_{xx}\overline{\rho} + \left(1.41\frac{C_{10}}{qC_{30}} + \frac{1.05}{qC_{30}} + 0.28\eta_0\right)\partial_t\overline{\rho}\right]. \tag{15}$$

Introducing the scaling $x=y\sqrt{3.31C_{20}/qC_{30}}$, $t=\tau\sqrt{3.31C_{20}/qC_{30}}$, $\overline{\rho}=4u/e\sqrt{3}$ and defining $\varepsilon=(4-\lambda)/e^2$ and $\mu=(1.41C_{10}/qC_{30}+1.05/qC_{30}+0.28\eta_0)/\sqrt{3.31C_{20}/qC_{30}}$, the equation reads

$$\partial_{tt}u = \partial_{xx}(\varepsilon u + u^3 - \partial_{xx}u + \mu\partial_t u), \tag{16}$$

which is the *van der Waals normal form* [3], where ε is the control parameter that is proportional to $\lambda-4$. When $\lambda<4$ the parameter ϵ is positive and the term proportional to it is a convective one. For $\lambda>4$ this term is a focusing one, that is, it increases the gradient and focuses the density in some spatial region. The term proportional to u^3 is a nonlinear convective one, the linear term with highest spatial derivative is a superconvective term, and the last term is diffusive. μ is the effective viscosity coefficient composed of the initial viscosity term η and the diffusion generated by the mechanical work. The terms of the above model are the dominant ones. One can check this by means of the scaling $u\sim\epsilon^{1/2}$, $v\sim\epsilon$, $\partial_x\sim\epsilon^{1/2}$, $\partial_t\sim\epsilon$, $\mu\sim o(1)$, and show that the other terms are negligible for small bifurcation parameter ($\epsilon\ll1$). Equation (16) is of order $\epsilon^{5/2}$. It can directly be checked that this scaling allows one to consider simultaneously both the linear and nonlinear terms in the equation. The first one gives rise to the instability and the second one is responsible for its saturation.

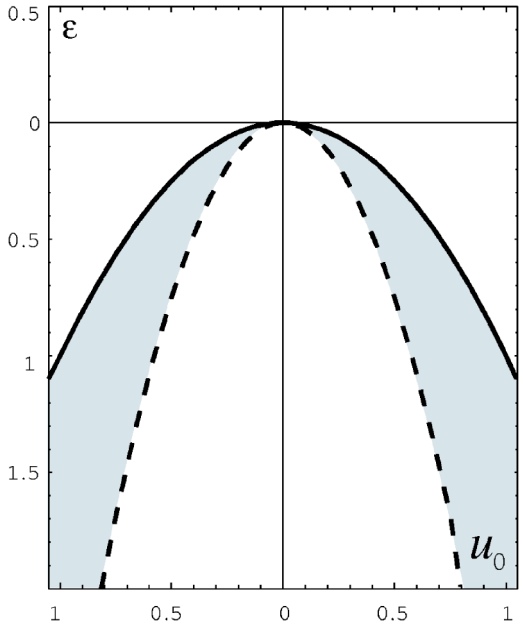

FIG. 5. Phase diagram obtained from the van der Waals normal form. The solid line (dashed) parabola is the metastable (spinodal) curve. The gray region is the bistability region.

It is important to note that the dynamics of the model (16) is characterized not only by the parameter $\{\epsilon, \mu\}$ but also by the parameter fixed by the initial condition

$$u_0 = \int dx u(x, t_0), \tag{17}$$

which follows from global mass conservation. One might think that the parameter $\int dx \partial_t u(x,t)|_{t_0}$ also characterizes the dynamics, but the resultant Galilean invariance allows us to set this parameter to zero. Hence the dynamics of this instability is characterized by three parameters $\{\epsilon, \mu, u_0\}$.

The van der Waals normal form can be written as

$$\partial_{tt} u = \partial_{xx} \frac{\delta \mathcal{F}}{\delta u} + \mu \partial_{xxt} u, \tag{18}$$

where $\mathcal{F} = \int dx \{\varepsilon u^2/2 + u^4/4 + (\partial_x u)^2/2\}$. The above dynamics can be regarded as the tendency of the system to minimize the Lyapunov functional

$$H = \int dx \left\{ \varepsilon \frac{u^2}{2} + \frac{u^4}{4} + \frac{(\partial_x u)^2}{2} + \frac{\partial_t \Lambda^2}{2} \right\}, \tag{19}$$

where Λ is an auxiliary functional defined as $\Lambda(x,t) \equiv \int^x dy u(y)/2$. Note that H satisfies

$$\frac{dH}{dt} = -\mu (\partial_t u)^2 \leqslant 0. \tag{20}$$

H is bounded and the minima of this Lyapunov functional are the minima of $\mathcal{F}$; hence the equilibrium states of Eq. (16) are the minima of $\mathcal{F}$ (for a detailed study of the properties of the functional $\mathcal{F}$, see Ref. [19]). The phase diagram of $\mathcal{F}$ is illustrated in Fig. 5, where the horizontal and vertical axes are u_0 and ϵ, respectively. The continuous line is the metastable curve and the dashed one is the spinodal curve. With periodic boundary conditions and initial mass u_0, $\mathcal{F}$ has two types of minima: the homogeneous and the bubble states as we describe in more detail below. Over the metastable curve in Fig. 5, the only minimum of $\mathcal{F}$ is the homogeneous state. In the region of parameters between the metastable and spinodal curve the minima of $\mathcal{F}$ are the homogeneous and the bubble states; one can observe this kind of solution from the metastable curve. Close to the metastable curve the homogeneous state is the global minimum, and close to the spinodal curve the bubble solution is the global minimum. Below the spinodal curve the bubble solution is the minimum of $\mathcal{F}$. We remark that as a consequence of the spatial translation invariance the bubble solution is parametrized by a symmetry group with one parameter, the position of the bubble.

V. DYNAMICS CLOSE TO THE CRITICAL POINT

In this section we analyze the dynamics close to the critical point, comparing the theoretical predictions that can be obtained from Eq. (16) and numerical solutions of the hydrodynamic model (4). For the purpose of comparison and to obtain numerical values, we have taken the transport coefficients C_1, C_2, C_3, and η to be constants, independent of the density. The values chosen are arbitrary, with the only precaution that the viscosity η must be small as it is observed in molecular dynamics simulations. These approximations simplify the analysis but do not qualitatively modify the character of the solutions.

The Lyapunov functional does not depend explicitly on the diffusion coefficient μ. Therefore this coefficient does not modify this phase diagram and the equilibrium states, but rather it changes the transient behavior exhibited by the system. For small μ, the transients are characterized by the presence of waves, while for large μ the transients are characterized by a diffusive behavior.

The region over the metastable curve is characterized by the stability of the homogeneous states and a perturbation of this state moves and spreads through the fluid. The dynamics of the normal form and the hydrodynamic model (4) are characterized in this region of parameters by dispersion and diffusion of sound waves. This is directly obtained by doing a linear analysis about the homogeneous state in Eq. (16) [20].

The region of parameters between the metastable and the spinodal curves is characterized by the coexistence of the homogeneous state and the bubble state (phase separation state), both being stable. Figure 6 shows the spatiotemporal diagram of the normal form, the hydrodynamic model (4), and the molecular dynamics simulation reported in [3]. When the homogeneous stable state initially is perturbed by a localized perturbation, this perturbation increases and saturates at a given density. Later, as seen in Fig. 6, two pairs of shock and rarefaction waves appear and move away, giving rise to the bubble. Due to the periodic boundary condition, the shock and rarefaction waves eventually collide, generating damped oscillations of the bubble as shown in Fig. 6. Hence, in this region of parameters, one can observe either the homogeneous state or the bubble solution, depending on

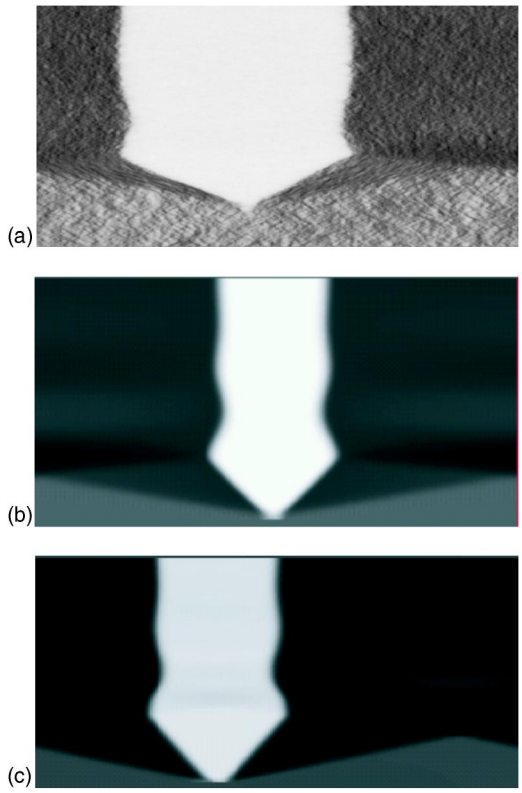

FIG. 6. Spatiotemporal evolution of the density, with time running up. The gray scale is proportional to density, with darker regions representing denser regions in the system. The top graph corresponds to a molecular dynamics simulation. The system size is 5400 and the total simulation time is $T=3.5\times10^5$. An initial condition (with $u=1.4\times10^{-2}$) that overcomes the nucleation barrier is imposed. The minimum (light gray) and maximum (dark gray) densities are $u=-2.6\times10^{-2}$ and $u=2.9\times10^{-2}$, respectively. The middle graph is obtained from the one-dimensional hydrodynamic model (4) with $C_{10}=0.38$, $C_{20}=0.37$, $C_{30}=10$, $P_0=1$, $\eta_0=0.0036$, $\lambda=4.5$, and $\rho=0.7$, where the system size is 200 and the total simulation time is $T=2000$. The minimum (light gray) and maximum (dark gray) densities are $\rho=0.12$ and $\rho=0.61$, respectively. The bottom graph is obtained from the model defined by Eq. (16) with $\varepsilon=-0.5$, $\nu=2$, and initial density $u(x,t=0)=0.43$, where the system size is 200 and the total simulation time is $T=800$. The minimum (light gray) and maximum (dark gray) densities are $u=-0.7$ and $u=0.7$, respectively.

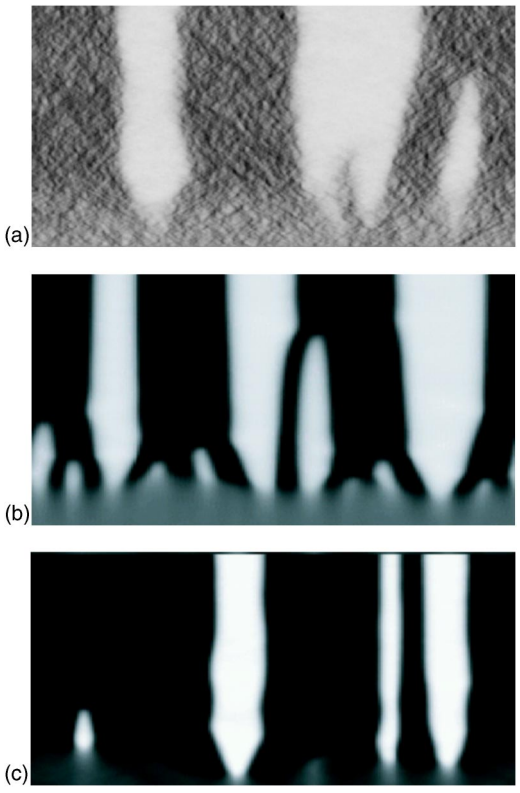

FIG. 7. Spatiotemporal evolution of the density, with time running up. The gray scale is proportional to the density, with darker regions representing denser regions in the system. The top graph corresponds to a molecular dynamic simulation. The system size is 5400 and the total simulation time is $T=1\times10^5$. The middle graph is obtained from the one-dimensional hydrodynamic model (4) with $C_{10}=0.38$, $C_{20}=0.37$, $C_{30}=10$, $P_0=1$, $\eta_0=0.0036$, $\lambda=4.5$, and $\rho=0.6$, where the system size is 100 and the total simulation time is $T=2000$. The minimum (light gray) and maximum (dark gray) densities are $\rho=0.32$ and $\rho=0.81$, respectively. The bottom graph is obtained from the van der Waals normal form (16) with $\varepsilon=-0.5$, $\nu=2$, and initial density $u(x,t=0)=0.35$, where the system size is 200 and the total simulation time is $T=800$. The minimum (light gray) and maximum (dark gray) densities are $u=-0.7$ and $u=0.7$, respectively.

the initial condition. It is important to note that the homogeneous state and bubble state are divided by a nucleation barrier that corresponds to an unstable bubble state. This unstable solution is nucleated by a saddle-node bifurcation with the stable bubble in the metastable curve [23,24].

Below the spinodal curve, the homogeneous state undergoes a spatial instability and the dynamical evolution is initially characterized by the appearance of spatial modulations. Later, this spatial modulation becomes a gas of bubbles that merge together, giving rise to a coarsening process. The transient of this coarsening process is different in the case of large or small viscosity (μ). For small viscosities, the transport of mass is through nonlinear waves (shock and rarefaction). Closer bubbles merge into a bigger one giving rise to a coalescence process. Subsequently, the bubble dynamics is led by an interaction mediated by sound waves (cf. Fig. 7), that is, mass and momentum are exchanged between bubbles by waves. For large viscosities the transients do not exhibit waves and the transport of mass is through the interaction of the bubbles, where the greatest bubbles grow and the smallest shrink. A study of this coarsening process and wave dynamics is in progress. It is important to remark that this process is less efficient than the transport of mass due to waves; hence the coarsening process is slower.

VI. STATIONARY SOLUTIONS OF THE NORMAL FORM

The equilibrium solutions of Eq. (16) with periodic boundary conditions obey the equation

$$-u+u^3-\partial_{xx}u-\lambda_0=0, \tag{21}$$

where λ_0 is an integration constant, that characterizes the stationary solutions. Due to the symmetry $\lambda_0\rightarrow-\lambda_0$ and u

$\rightarrow -u$, we will assume, without loss of generality, that λ_0 is positive. The above Newton type of equation is integrated into

$$V(u) + (\partial_x u)^2 = E \tag{22}$$

where the potential energy is $V(u) = 2\lambda_0 u + \varepsilon u^2 - u^4/2$. The potential $V(u)$ has three extrema if $\lambda_0^2 < \lambda_c^2$, $\lambda_c \equiv 2/(3\sqrt{3})$. We will denote them $u_a \leqslant u_b \leqslant u_c$, and they have the form

$$u_a = -2\sqrt{\frac{|\varepsilon|}{3}}\sin\left(\frac{1}{3}\arctan\sqrt{\frac{4|\varepsilon|}{27\lambda_0^2} - 1} + \frac{\pi}{6}\right), \tag{23}$$

$$u_b = 2\sqrt{\frac{|\varepsilon|}{3}}\sin\left(\frac{1}{3}\arctan\sqrt{\frac{4|\varepsilon|}{27\lambda_0^2} - 1} - \frac{\pi}{6}\right), \tag{24}$$

$$u_c = 2\sqrt{\frac{|\varepsilon|}{3}}\cos\left(\frac{1}{3}\arctan\sqrt{\frac{4|\varepsilon|}{27\lambda_0^2} - 1}\right). \tag{25}$$

Note that $|\varepsilon|/3 < u_{a,c}^2 < 1$, and $-\sqrt{|\varepsilon|/3} < u_b < 0$. In the case of infinite size ($L_x \gg 1$) the phase diagram of the Newton type equation has a bubble or homoclinic solution, which starts at u_a, later moves to u_c, and finally comes back to u_a. The analytic expression of this solution is

$$U(x - x_0) = u_a + \frac{2(3u_0^2 + \varepsilon)}{-2u_0 + \sqrt{2(|\varepsilon| - u_0^2)}\cosh[\sqrt{(3u_0^2 + \varepsilon)}x - x_0]}, \tag{26}$$

In the case of Neumann boundary conditions, that is, $\partial_{xx} u = \partial_{xxxx} u = 0$, the bubble solution is not the global minimum and it is replaced by the wall or kink solutions

$$U(x - x_0) = \mp\sqrt{|\varepsilon|}\tanh\left(\sqrt{\frac{|\varepsilon|}{2}}(x - x_0)\right). \tag{27}$$

This solution represents physically a coexistence between two phases with only one interface between the phases. The bubble solution has two interfaces; therefore it is energetically more costly. The dynamics in this case is similar to that with periodic boundary conditions, and the main difference is that the bubble solution moves to the nearest boundary and finally gives rise to the wall or kink solution.

VII. DISCUSSION OF HYDRODYNAMIC SOLUTIONS IN TWO DIMENSIONS AND CONCLUSIONS

We have studied a one-dimensional hydrodynamic model that mimics a two-dimensional fluidized granular system with a vibrating wall and without gravity, which exhibits a phase separation. Close to the critical point, we have deduced the van der Waals normal form (16). The choice of the hydrodynamic model is based on its simplicity, which captures most of the dynamics near the onset of the instability in two spatial dimensions, and also because its simplicity allows for a detailed analytic study. The adiabatic elimination of the temperature allows us to understand the origin of the effective viscosity, which is a combination of the hydrodynamic viscosity η and the heat generated by the mechanical

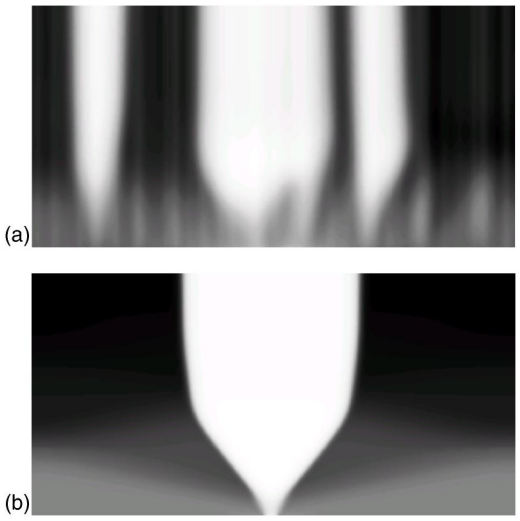

FIG. 8. Spatiotemporal evolution of the density given by the numerical solution of the full two-dimensional hydrodynamic equations. Time is running up, and the gray scale is proportional to the density, with darker regions representing denser regions in the system. In both graphs, the common parameters are $L_x = 100\,000$, $L_y = 100$, $T_W = 1$, and $\rho = 0.11$. In the top graph, the inelasticity coefficient is $q = 0.01$ and an initial noise is added to produce unstable bubbles. In the bottom graph, $q = 0.015$, an initial nucleus grows with the emission of two shock waves.

work. The linear spatial saturation at the onset of the bifurcation is related to the fact that the density gradients locally increase the temperature, breaking the tendency to focus the grains.

In the original two-dimensional problem, it is difficult to make a complete analysis like the one performed here, but it is important to verify if the conclusions of this work are valid in two dimensions. Using the full hydrodynamic equations for the density, momentum, and temperature fields, some conclusions can be extracted in two dimensions. It has been shown, using numerical solutions of the hydrodynamic equations, that they present a region in parameter space where the longitudinal compressibility becomes negative [20–22]. In Ref. [20] the spinodal and coexistence curves were deduced numerically. The numerical character of the solutions, however, does not allow for a derivation of the normal form associated with the instability, but the arguments presented in [3] indicate that the van der Waals normal form is the appropriate model. Also, to make a qualitative comparison of the phenomena predicted by the van der Waals normal form to the two-dimensional system, we have numerically solved the full hydrodynamic equations in two dimensions for dense granular fluids. We consider hydrodynamic equations for dense quasielastic granular fluids, which are similar to the equations for elastic compressible fluids, with the addition of an energy sink term (see [14,15]). The transport coefficients are those of the quasielastic inelastic hard sphere model, and the full set of equations and coefficients are given in [15,20]. The equations are solved using a finite volume approach with a small time step in order to take into account both the hyperbolic (sound and compressible effects) and parabolic (viscosity and heat transfer) parts of the equations with high

precision. The system under study has a vibrating wall, but for computational feasibility we model it using a thermal wall at temperature T_W. The other boundary conditions are the same as those of the system under study.

In the hydrodynamic description, this implies that the temperature of the granular fluid is imposed to be T_W by the wall. This boundary condition fails to reproduce exactly the molecular dynamics simulations, where a temperature jump is observed in the Knudsen layer [20]. The initial conditions are those of a fluid at rest with uniform density and the temperature given by the wall, where the global density is chosen to be in the metastable or unstable region, according to the results presented in Ref. [20]. The initial condition evolves fast to a horizontally homogeneous state with the y dependence given by the energy and momentum balance [14]. After the transient, the observed phenomena (see Fig. 8) are similar to those deduced from the normal form and observed in molecular dynamics simulations: waves, shocks, instability, metastability, and bubbles. One difference is that the viscosity seems to be larger than in molecular dynamics simulations, implying a faster attenuation of the shock waves. It is important to note that, although these phenomena are found in the two-dimensional system, the full equations are so intricate that it is difficult to predict them compared with the normal form.

ACKNOWLEDGMENTS

The authors thank P. Cordero, S. Rica, and E. Tirapegui for fruitful discussions. The simulation software developed at INLN, France, has been used for the simulations of model (16) and (4). The simulations of the two-dimensional hydrodynamic model were done in the parallel cluster of CIMAT. M.G.C. and R.S. acknowledge the support of FONDAP Grant No. 11980002. M.G.C. and R.S. are very grateful for the support of FONDECYT Projects No. 1020782 and No. 1030993, respectively. C.C. acknowledges the support of a DIPUC grant.

[1] E. Livne, B. Meerson, and P. V. Sasorov, Phys. Rev. E **65**, 021302 (2002).
[2] J. J. Brey, M. J. Ruiz-Montero, F. Moreno, and R. García-Rojo, Phys. Rev. E **65**, 061302 (2002).
[3] M. Argentina, M. G. Clerc, and R. Soto, Phys. Rev. Lett. **89**, 044301 (2002).
[4] L. D. Landau and E. M. Lifshitz, *Statistical Physics* (Pergamon, New York, 1969).
[5] I. Goldhirsch and G. Zanetti, Phys. Rev. Lett. **70**, 1619 (1993).
[6] P. Zamankhan, A. Mazouchi, and P. Sarkomaa, Appl. Phys. Lett. **71**, 3790 (1997).
[7] D. C. Rapaport, Physica A **249**, 232 (1998).
[8] J. T. Jenkins and M. W. Richman, Arch. Ration. Mech. Anal. **87**, 355 (1985).
[9] T. Jenkins and M. W. Richman, J. Fluid Mech. **192**, 313 (1988).
[10] J. J. Brey, F. Moreno, and J. W. Dufty, Phys. Rev. E **54**, 445 (1996).
[11] N. Sela, I. Goldhirsch, and S. H. Noskowicz, Phys. Fluids **8**, 2337 (1996).
[12] J. J. Brey, J. W. Dufty, C. S. Kim, and A. Santos, Phys. Rev. E **58**, 4638 (1998).
[13] D. Risso and P. Cordero, Phys. Rev. E **65**, 021304 (2002).
[14] E. L. Grossman, T. Zhou, and E. Ben-Naim, Phys. Rev. E **55**, 4200 (1997).
[15] V. Garzó and J. W. Dufty, Phys. Rev. E **59**, 5895 (1999).
[16] Y. Du, H. Li, and L. P. Kadanoff, Phys. Rev. Lett. **74**, 1268 (1995).
[17] D. Henderson, Mol. Phys. **30**, 971 (1975).
[18] P. Berge, Y. Pomeau, and Ch. Vidal, *Order within Chaos: Towards a Deterministic Approach to Turbulence* (Wiley, New York, 1984).
[19] J. D. Gunton, M. San Miguel, and P. Sanhi, in *Phase Transitions and Critical Phenomena*, Vol. 8, edited by D. Domb and J. L. Lebowitz (Academic, London, 1983), pp. 267–466.
[20] M. Argentina, M. G. Clerc, and R. Soto, in *Granular Gas Dynamics*, edited by T. Pöschel and N. Brilliantov, Lecture Notes in Physics Vol. 624 (Springer, Berlin, 2003).
[21] E. Khain and B. Meerson, Phys. Rev. E **66**, 021306 (2002).
[22] J. J. Brey, F. Moreno, R. García-Rojo, and M. J. Ruiz-Montero, Phys. Rev. E **65**, 011305 (2002).
[23] M. Argentina, M. G. Clerc, R. Rojas, and E. Tirapegui (unpublished).
[24] A. Novick-Cohen and L. A. Peletier, Proc. - R. Soc. Edinburgh, Sect. A: Math. **123**, 1071 (1993).